

Cooling history and exhumation of the Nepheline Syenites, NW Iran: Constraints from Apatite fission track

Nasser Ashrafi*¹, Noriko Hasebe², Ahmad Jahangiri³

1. Department of Geology, Payame Noor University, P.O. Box 19395-3697 Tehran, Iran

2. Institute of Nature and Environmental Technology, Kanazawa University, Japan

3. Department of Geology, Natural Science Faculty, University of Tabriz, Iran

Received 20 September 2017; accepted 5 February 2018

Abstract

Thermal history and apatite fission-track ages were determined for the Kaleybar, Razgah and Bozqush alkaline intrusions which display Eocene-Oligocene stratigraphic age. These subduction-related intrusions are located in the Alborz-Azerbaijan magmatic belt which is characterized by a Paleogene magmatic flare-up associated with extensional/transensional tectonism. The mean of Uranium content and apparent age for apatites of the Bozqush, Kaleybar, and Razgah were obtained 21.8 (± 3.8), 9.5 (± 5.7), and 24.5 (± 11.3) ppm and 29 (± 1.8), 36.6 (± 3.0), and 40.7 (± 1.3) Ma (σ), respectively, which represented the time that the rocks of intrusions were last at temperatures of 60 °C to 110 °C. The results indicate that the apatite apparent ages are in concord with the stratigraphic ages. The apatite fission track ages and track lengths distribution were combined to construct time-temperature history by inverse modeling, which represented the all samples resided in the partial annealing zone (PAZ) for a significant period of time. The apatite fission track analysis indicated relatively complex cooling history for the host rocks because of the magmatic activity, as it was occurred during Cenozoic in the Alborz-Azerbaijan magmatic belt. The time-temperature curves of the studied intrusions begun with a relatively rapid initial cooling and followed by long residence at the PAZ temperature (heating stage). The time-temperature paths indicate that the start of rapid recent cooling to the surface temperatures was occurred at 5 Myrs.

Keywords: Thermal history, Nepheline syenite, Bozqush, Razgah, Kaleybar

1. Introduction

Fission-track chronometry is widely used to establish both age and thermal history in a wide variety of geological applications (e.g. Green et al. 1989; Gallagher et al. 1994; Fitzgerald et al. 1995; Carter 1999; Kohn and Green 2002). Applicable geological settings include orogenic belts, rifted margins, faults, sedimentary basins, cratons, and mineral deposits. The types of geologic problems that can be addressed include the timing and rates of tectonic events, sedimentary basin evolution, the timing of hydrocarbon generation and ore mineralization, the absolute age of volcanic deposits, the effects of major climatic changes on the near-surface geothermal gradient, and long-term landscape evolution (Donelick et al. 2005). Apatite is widely employed in low temperature thermochronology studies with the apatite fission track and apatite (U-Th)/He thermochronometers yielding thermal history information in the 60–110°C (Laslett et al. 1987) and 55–80°C (Farley 2000) temperature windows, respectively. Apatite has also been employed in high temperature thermochronology studies, which demonstrate that the U–Pb apatite system has a closure temperature of ca. 450–550°C (Chamberlain and Bowring 2000; Schoene and Bowring 2007). Apatite U–Pb age information can also be supplemented by low

temperature thermochronometric techniques on the same crystals to constrain the exhumation history of the grains. Apatite has also been used in Lu–Hf geochronology studies (Barfod et al. 2003) and as an Nd isotopic tracer (Foster and Vance 2006; Gregory et al. 2009).

Conventionally in the fission-track chronometry, uranium concentration is determined using a neutron activation technique to induce fission in a proportion of ²³⁵U atoms, recording the fission events in an external detector to give essentially a map of uranium distribution (e.g. Gleadow 1981; Hurford and Green 1982). Laser Ablation-Inductively Coupled Plasma-Mass Spectrometry (LA-ICP-MS) is an alternative method for direct measurement of uranium concentrations for determination of single-grain fission-track ages (e.g. Cox et al. 2000; Svojtka and Kosler 2002; Hasebe et al. 2004; Chew and Donelick 2012; Hasebe et al. 2013). LA-ICP-MS has been used widely to measure the chemical composition of small amounts of solid samples in many fields (e.g. environmental, geological, and archeological sciences). The methodology does not require special sample preparation such as sample dissolution and carbon film coating, and is therefore time efficient. The subduction of Neo-Tethys beneath Iranian plate during the Late-

*Corresponding author.

E-mail address: n_ashrafi@pnu.ac.ir

Cretaceous to Paleogene and following continent–continent collision of Iranian and Arabian plate was responsible for developing the ribbon structural zones in Iran (Fig 1) (e.g. Mohajjel et al. 2003). The NW-trending Alborz-Azerbaijan Magmatic Belt (AAMB) that stretches from the Alborz Mountains to Azerbaijan Province is separated from the Urumieh-Dokhtar Magmatic Arc (UDMA) to the south by the Tabriz Fault (Alavi 1996). The AAMB has a complex successive extension and collision history during Cenozoic.

Thermal history studies of the AAMB are rare (Axen et al. 2001; Guest et al. 2006; Rezaeian et al. 2012; Ballato et al. 2013). Axen et al. (2001) have been indicated that the Alam Kuh region from Late Eocene to Late Miocene time was tectonically stable and the Akapol suite had 0.7 km/m.y. exhumation between 6 and 4 Ma. Rezaeian et al. (2012) suggested enhanced exhumation ca. 35±5 Ma, minor exhumation between ca. 30–20 Ma and an increase in exhumation thereafter for the Alborz Mountains.

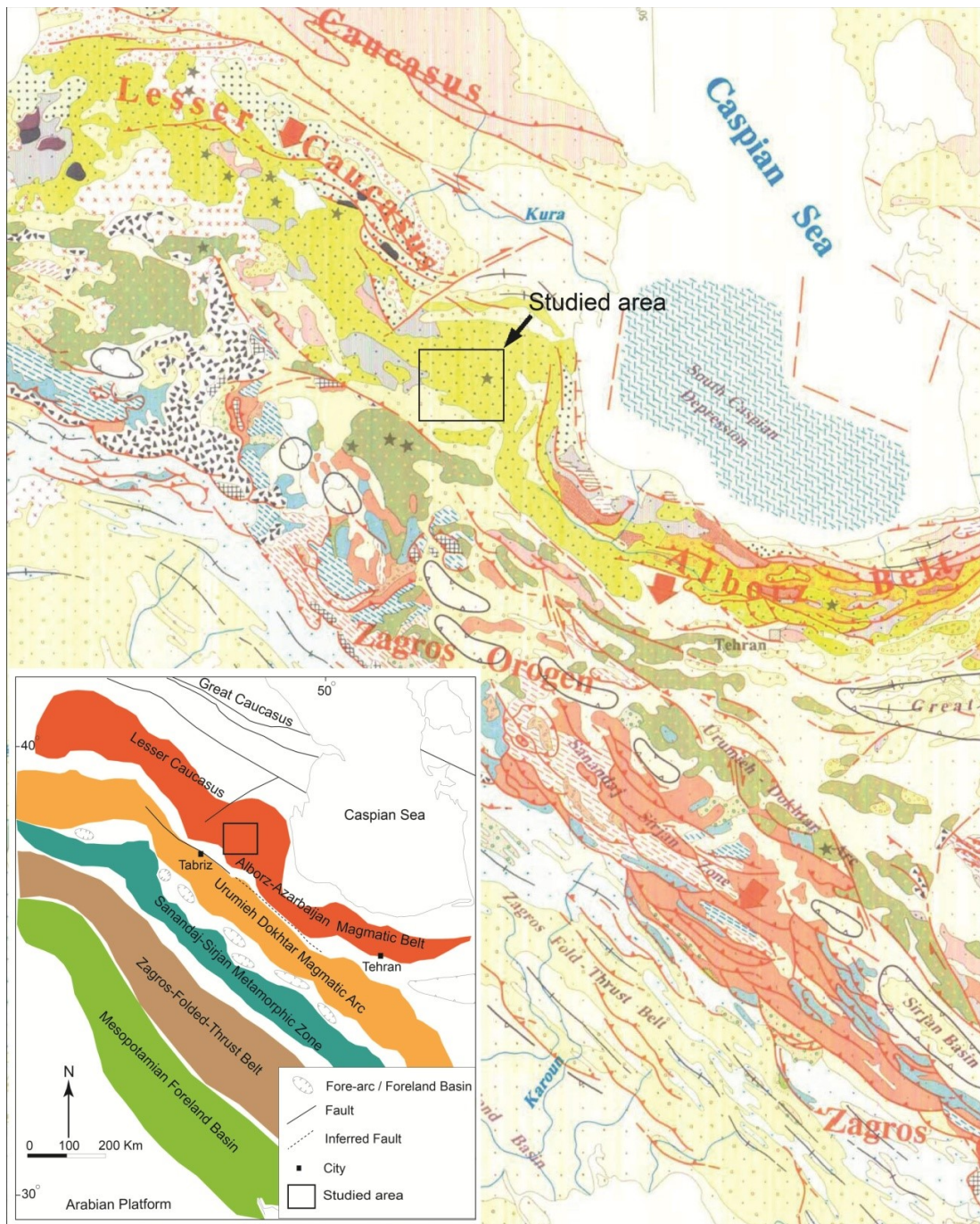


Fig 1. A part of the Tectonic Map of Middle East (Alavi 1991) showing the location of studied area in the important Iranian structural-magmatic zones. Inset: A simplified structural map showing the main geological units of Iran, the rectangle represents the situation of studied plutons.

The apatite fission track (AFT) of the Kaleybar, Razgah and Bozqush (KRB) feldspathoid syenites has been studied with the aim of determining the cooling history and the apparent age. They are located in East Azerbaijan province of Iran and the geological zone of the AAMB (Fig 1 and 2). The KRB sub-volcanic intrusions were formed by the Eocene-Oligocene magmatism, which was dominant in volume in NW Iran (Babakhani et al. 1990). Mineralogy, petrology, and

geochemistry of the KRB intrusions have been studied by some researchers (e.g. Moine-Vaziri 1999; Ashrafi 2004; Ashrafi 2009; Tajbakhsh et al. 2012). However, there is no data on thermochronology and geochronology of the KRB. These intrusions were selected for AFT studies because they were related to a same magmatic cycle, i.e. Eocene-Oligocene shoshonitic cycle; also they had abundant and proper apatite grains for fission track analysis.

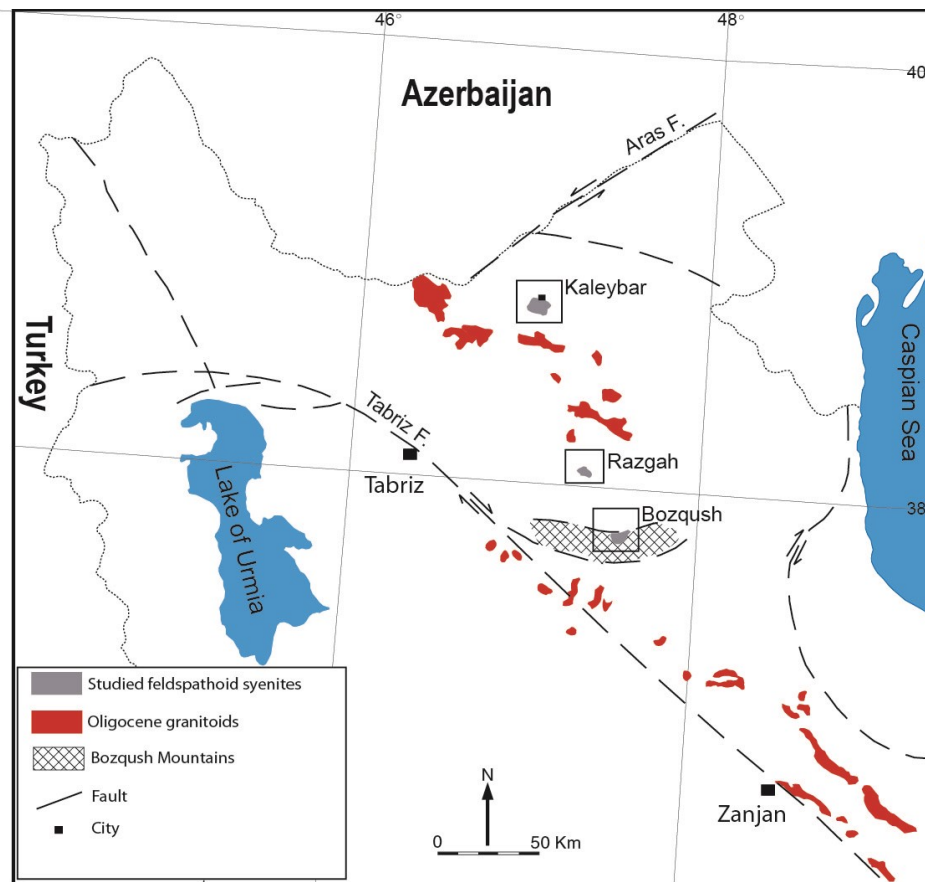


Fig 2. Map of Eocene-Oligocene plutonism in NW Iran with location of the Kaleybar, Razgah, and Bozqush plutons, shown as squares (simplified and modified from Aghanabati, 1990).

2. Geological setting

Extensive magmatism activity has occurred in the NW Iran from Cretaceous to Quaternary that can be divided to four main cycles (Stöcklin and Nabavi 1973; Alberti et al. 1976; Didon and Gemain 1976; Comin-Chiaromonti et al. 1979; Ghorbani 2011):

The first from Late Cretaceous to Early Eocene, this is mainly characterized by volcanic rocks as well small sub-volcanic intrusions. The magmatism was first submarine and then subaerial (e.g. Comin-Chiaromonti et al. 1979). It has limited areal extent and was characterized by a strong explosive activity. The second from Eocene to Oligocene, this magmatic (shoshonitic-alkaline) cycle is characterized by many granitic-syenitic-gabbroic stocks/batholiths (e.g. Castro et al. 2013; Mollai et al. 2014; Nabatian et al. 2014). The

most abundant volcanic rocks are Ne-normative tephritic lavas in which the foids are mainly represented by analcime (analcime-bearing tephritic phonolites). The third magmatic cycle from Miocene to Pliocene, which is characterized by moderately alkaline and foid-free volcanic rocks (9-11 Ma; Alberti et al. 1976) and small intrusions; Products of this volcanism range from latitic rocks to alkali-quartz trachytes (Comin-Chiaromonti et al. 1975, 1978; Jahangiri 2007). Limited occurrences of Miocene analcime/leucite-bearing alkaline volcanics are also reported from the NW Iran (Shafaii-Moghadam et al. 2014). The fourth magmatic cycle, Plio-Quaternary volcanism, displays sub-alkaline, high-K calc-alkaline and alkaline affinities (e.g. Ahmadzadeh et al. 2010; Dabiri et al. 2011).

The KRB shallow-level intrusions were formed by the second magmatic cycle. The Kaleybar pluton intruded into Late-Cretaceous limestones and intermediate to acidic lava flows. There are distinct contact metamorphism areoles and chilled margin around the Kaleybar pluton. The Kaleybar pluton mainly consists of nepheline syenite and gabbro. A gradual change from nepheline syenite to gabbro is observed locally. Also, pyroxenite as enclave and lenticular small body in and/or near the gabbro occurred in the southern of the pluton. Furthermore, small intrusions with syenite and quartz monzonite compositions took place in the northern and center of the Kaleybar pluton. Based on the field evidences such as the enclaves, intrusive contacts, and apophyses within the Kaleybar pluton, the pyroxenite and gabbro are older than the nepheline syenite and quartz monzonite. The general textures of the main rocks are coarse-grained granular and porphyritic. They have been mostly cut by abundant pink-coloured aplitic and pegmatitic dykes. Also, gabbroic and phonolitic dykes were occurred in the Kaleybar pluton (Ashrafi 2009).

The Razgah pluton is in contact with Quaternary sediments. However, there are Eocene and Miocene basaltic andesite and gypsiferous marl in the vicinity of the Razgah pluton. The Razgah pluton composition varies from pseudoleucite syenite to monzo-diorite/syenite. The contact between the pseudoleucite syenite and monzo-diorite/syenite is typically controlled by faulting, however a gradual change is observed locally. The pseudoleucite syenites have porphyritic texture with pseudoleucite megacrysts, whereas monzo-diorites/syenites have coarse-grained texture. They have been cut by abundant pink-coloured micro-syenitic, micro-granitic, and pegmatitic dykes as well dark grey phonolitic dykes up to 4 meters in thickness. Also, the Razgah pluton is cut by aplitic and silicic dykes in the west margin, where copper mineralization is associated with the dykes.

The Bozqush pluton intruded into the Eocene megaporphyry andesite, analcime trachy-andesite, trachyte, and tuff. The slight contact metamorphism areole and chilled margin are observed in the eastern and the western of the Bozqush pluton respectively. The main rocks of the Bozqush pluton consist of biotite nepheline syenite and pseudoleucite syenite. The pseudoleucite syenite forms a small part and occurs in the southern of the pluton. The Bozqush pluton is mostly cut by abundant aplitic and pegmatitic dykes up to 5 meters thickness. The dykes vary from syenite to granite in composition and are light pink to light grey in colour. Also dark grey basaltic dykes occur scarcely.

3. Petrography

3.1. Kaleybar intrusion

According to the recommendations of the International Union of Geological Sciences (IUGS) (Le Maitre et al.

2002), the Kaleybar intrusion consist of nepheline-bearing alkali-syenite, nepheline-bearing syenite, nepheline syenite, nepheline-bearing monzonite, nepheline-bearing monzodiorite, nepheline-bearing diorite/gabbro, quartz monzonite, quartz-monzo diorite, monzo-diorite, quartz-alkali syenite, and clinopyroxenite. The rock forming minerals are alkali-feldspar, nepheline, plagioclase, amphibole (up to 10%), clinopyroxene (up to 5%), melanite (up to 5%), biotite, apatite, titanite, zircon, spinel, Fe-Ti oxide, quartz, and secondary minerals (including sericite, muscovite, sodalite, analcime, cancrinite, zeolite, epidote, chlorite, quartz, calcite, iron oxide, and clay minerals). Melanite and feldspathoids, including nepheline, analcime, and sodalite, take place in the silica-undersaturated rocks. Quartz occurs in the silica-oversaturated rocks. Spinel only appears in clinopyroxenite with a Fe-Ti oxide margin.

3.2. Razgah intrusion

The Razgah pluton consists of pseudoleucitolite (more than 60% pseudoleucite), pseudoleucite monzo-syenite, and pseudoleucite/nepheline monzo-diorite, and nepheline monzo-syenite. The pseudoleucite syenite and nepheline monzo-syenite constitute the main bulk of the pluton. The pseudoleucitolite and pseudoleucite syenite are coarse-grained and porphyritic with pseudoleucite megacrysts up to 5 cm across. The rock forming minerals of the main rocks are pseudoleucite, alkali-feldspar, plagioclase, clinopyroxene (up to 10%), nepheline, olivine (up to 5%), biotite, apatite (up to 2%, Fig 3a), zircon, Fe-Ti oxide, and secondary minerals (including zeolite, calcite, iron oxide, sericite, muscovite, analcime, iddingsite, chlorite, quartz, and clay minerals).

3.3. Bozqush intrusion

The Bozqush intrusion consists of nepheline-bearing biotite syenite, nepheline monzo-syenite, nepheline-bearing monzo-syenite, nepheline-bearing monzo-diorite, and pseudoleucitolite. The rock forming minerals are alkali-feldspar, plagioclase, biotite (up to 10%), clinopyroxene (up to 5%), nepheline, amphibole, melanite, olivine, apatite, titanite, zircon, Fe-Ti oxide, pseudoleucite, and secondary minerals (including sericite, muscovite, analcime, zeolite, epidote, quartz, calcite, and clay minerals). The alkali-feldspar generally shows microperthitic and poikilitic texture. The plagioclase occasionally shows a distinct compositional zoning. The biotite is the main hydrous mineral and occurs as individual grains and/or around the Fe-Ti oxides. However, the amphibole happens at the margin of some clinopyroxene grains. Fine-grained melanite garnet (up to 1%) only appears in a sample from the margin of the pluton.

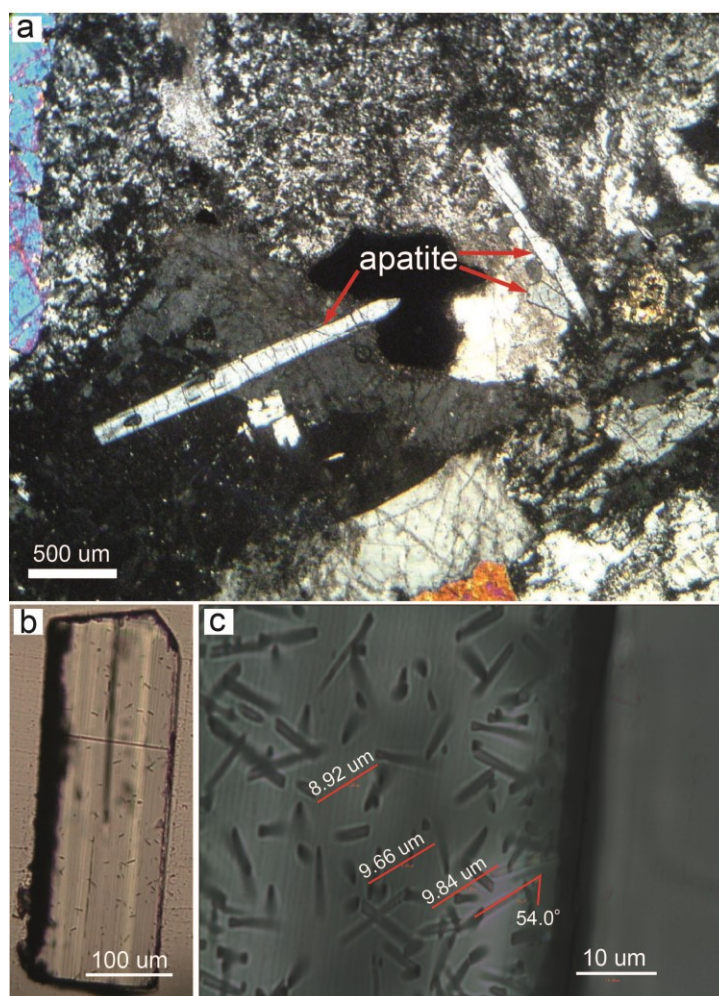


Fig 3. Photomicrographs of the apatite crystals from the Razgah pluton. (a) The elongated and abundant apatites in pseudoleucite syenite. (b) Etched fission tracks in the apatite under plane transmitted light. (c) Measurement of confined fission track length and its angle to the c-axis.

4. Materials and Methods

After the petrography studies, rock samples in weight 500 g to 2.5 kg from the intrusions of Kaleybar (nepheline syenite), Razgah (pseudoleucite syenite) and Bozqush (nepheline syenite) were collected for mineral separation. Fission track analysis was accomplished in Geochronology group, Kanazawa University, Japan. The following steps were carried out to separate the minerals required for analysis: (1) samples crushing to achieve grains <0.5 cm in diameter; (2) using the method of sieving separation to obtain particles <250 μm ; (3) separation of ferromagnetic and non-ferromagnetic minerals (e.g. magnetite, biotite, hornblende, pyroxene, ilmenite, epidote); (4) The non-magnetic fraction that contains datable minerals such as apatites and zircons (plus feldspar, feldspathoid, etc) is then subjected to heavy liquid separations; therefore, a mixture of minerals was placed in the separatory funnel with the heavy liquid of LST (density= $2.85 \pm 0.02 \text{ g/cm}^3$); and (5) In this step, 450 proper apatite grains were achieved through hand-picking individual grains using an optical binocular microscope (Nikon SMZ

645). Small fraction of the handpicked apatite grains was spread on a silica glass slide and embedded in epoxy resin. Next, the exposed surface of grains were ground and polished with a sand paper and diamond paste using standard techniques. The separated apatites were etched chemically in 5M HNO_3 at $20 \pm 1^\circ\text{C}$ for 20s (Fig 3b, 3c). Then, track lengths and densities were determined using digital camera Focus Studio 2100 connected with an optical microscope (NIKON ECLIPSE E600).

Uranium measurements were carried out using LA-ICP-MS. Analysis was made at the Agilent 7500s ICP-MS facility, Kanazawa University, using a MicroLas GeoLas Q plus (wavelength 193 nm) laser. Repetition rate and pit diameter were 5 Hz and $\sim 20 \mu\text{m}$, respectively. ^{238}U concentrations were calibrated against NIST 610 and NIST 612 standard glasses (Pearce et al. 1997). In total six datasets were provided for a whole measurements. One dataset contains three measurements for each standard glass. Data reduction was carried out in Microsoft Excel. ^{44}Ca was used as an internal

standard using chemical data obtained previously (e.g. Jarvis and Williams 1993; Barbarand et al. 2003).

The fission-track age equation for using in the LA-ICP-MS method has been extracted as following (Hasebe et al. 2004):

Total uranium concentration of apatites ($\mu\text{g/g}$) was calculated from measured ^{238}U content ($\mu\text{g/g}$) and natural isotope abundance ratio of uranium (^{235}U : 0.71% / ^{238}U : 99.29% in weight), making the reasonable assumption of a natural $^{235}\text{U}/^{238}\text{U}$ ratio in all apatite samples. Therefore

$$U = \frac{^{238}\text{U}}{^{238}\text{U} + ^{235}\text{U}} A \quad (1)$$

where U = sample total uranium content ($\mu\text{g/g}$), ^{238}U = uranium-238 content ($\mu\text{g/g}$) obtained from LA-ICP-MS, and A_{238} = abundance of ^{238}U in weight (0.9929).

The general age equation is:

$$D_t = \frac{\lambda_f}{\lambda_D} N_{238} (e^{\lambda_D t} - 1) \quad (2)$$

where D_t = number of decay events of ^{238}U during time t in a unit volume (cm^{-3}), λ_f = ^{238}U spontaneous fission decay constant ($8.46 \times 10^{-17} \text{ year}^{-1}$ Spadavecchia and Hahn 1967), λ_D = ^{238}U total decay constant ($1.55125 \times 10^{-10} \text{ year}^{-1}$ Jaffey et al. 1971), N_{238} = current number of uranium-238 atoms in a unit volume (cm^{-3}), and t = FT age (years). Because the number of fission decay events is observed as a spontaneous track density, the equation is changed to:

$$\rho_s = \frac{\lambda_f}{\lambda_D} N_{238} (e^{\lambda_D t} - 1) R_{sp} k \quad (3)$$

where ρ_s = spontaneous FT density at the observed surface (cm^{-2}), R_{sp} = a registration factor by which ^{238}U in a unit volume would leave spontaneous tracks on an observed surface (cm), and k = a constant, which would be variable depending on experimental factors such as etching and observation conditions. Here N_{238} (cm^{-3}) is calculated using the content of uranium-238:

$$N_{238} = N_A \cdot \frac{^{238}\text{U} \cdot 10^{-6} \cdot d}{M} \quad (4)$$

where N_A = Avogadro's number, ^{238}U = uranium-238 content measured by LA-ICP-MS ($\mu\text{g/g}$), d = apatite density (taken as 3.19 g/cm^3), and M = the mass of ^{238}U . Therefore,

$$t = \frac{1}{\lambda_D} \ln \left(1 + \frac{\rho_s \lambda_D M}{\lambda_f N_A ^{238}\text{U} 10^{-6} d R_{sp} k} \right) \quad (5)$$

In this study we adopted as R_{sp} a half of the mean etchable spontaneous fission-track length in apatite from geologically rapidly cooled samples without subsequent thermal disturbance ($7.5 \mu\text{m} = 7.5 \times 10^{-4} \text{ cm}$; Gleadow et al. 1986b), and k is set as 1. The error of a grain age is given by

$$\sqrt{\frac{1}{N_s} + \delta^2} \quad (6)$$

where N_s = the number of counted spontaneous tracks, and δ = uncertainties in uranium concentration (10% = 0.1). The depth of the ablated trench is estimated $25 \pm 5 \mu\text{m}$ by microscopic observation.

5. Results and discussion

As described above, by comparing the density of fission tracks with the U content of the mineral, an apparent fission track age can be calculated. The mean of U content for the apatites of Bozqush, Kaleybar, and Razgah are 21.8, 9.5, and 24.5 ppm, with the standard deviation of 3.8, 5.7, and 11.3, respectively. The densities of spontaneous tracks in the apatite grains vary from 0.2×10^6 – $0.5 \times 10^6 \text{ cm}^{-2}$. Based on the measured data and using the above described method, the mean apparent age for the apatites from the Bozqush, Kaleybar, and Razgah intrusions were calculated 29 (± 1.8), 36.6 (± 3.0), and 40.7 (± 1.3) Ma (σ), respectively. Also, a summary of the measured and calculated data is presented in Table 1.

Table 1. Fission-track apatite ages calculated by LA-ICP-MS method.

Apatite sample	No. of grains	$\rho_s, \times 10^6 \text{ cm}^{-2}$	N_s	U, ppm	U, SD	P (χ^2), %	t, Ma	σ
Bozqush	14	0.3	267	21.8	3.8	17.69	29.0	1.8
Kaleybar	18	0.2	145	9.5	5.7	1.88	36.6	3.0
Razgah	27	0.5	1021	24.5	11.3	1.82	40.7	1.3

Abbreviations: ρ_s = densities of spontaneous tracks cm^{-2} ; N_s = numbers of tracks counted for spontaneous measurements; U = average uranium content; SD = standard deviation; P(χ^2) probability of χ^2 for (n-1) degrees of freedom, n = number of grains (Galbraith 1981); t = weighted mean of grain ages; σ = error of ages

In addition to the fission track age, the apatite fission track method also yields information on the nature of the cooling path. This information is obtained from the distribution of confined fission track lengths in a sample (Gleadow et al. 1986a). Confined fission tracks are horizontal (or $<10^\circ$ from horizontal) tracks that lie in a c-axis prismatic section, such that both ends of the track are visible entirely within the polished and etched apatite crystal without altering the focal depth. The studied apatite grains exhibits a fission track population

with mean track lengths $11 \pm 1 \mu\text{m}$ (Table 2). Unannealed, spontaneous fission track lengths in natural apatite grains typically range between ~ 14.5 and $15.5 \mu\text{m}$ depending on its chemical composition (Gleadow et al. 1986a). Long mean confined track lengths ($>14 \mu\text{m}$) and narrow track length distributions indicate rapid cooling through the PAZ, whereas shorter mean values ($<14 \mu\text{m}$) or a wide range of track lengths generally indicate slower cooling or a complex cooling path (Gleadow et al. 1986b).

The fission track ages provide an estimate of the time that have elapsed since the mineral cooled through a specific temperature window (referred to as the partial annealing zone or PAZ). The apatite PAZ is estimated at 60–110°C although this varies with apatite composition (Green et al. 1986; Carlson et al. 1999; Barbarand et al. 2003). At temperatures higher than the PAZ, there is sufficient energy to completely anneal (or remove) fission tracks via thermally activated diffusion of the relocated ionic species in the lattice. At temperatures lower than the PAZ, there is insufficient energy to cause significant repair of fission tracks. Fission tracks are partially annealed at temperatures within the PAZ.

The apatite fission track age and track length distribution can be combined to construct time–temperature paths by inverse and/or forward modeling of the fission track age and length data (e.g. Gallagher 1995; Ketcham 2005). Forward modeling is resulted in model age based on relating fission-track length to fission-track density, whereas inverse modeling represents the range of possible thermal histories that are consistent with the measured data. There are a

number of the modeling software, such as AFTSolve and HeFTy (Ketcham et al. 2000; Ketcham 2005), that implements one or more of the thermochronometer systems. These programs vary not only in how they implement their forward and inverse modeling calculations, but in their overall approaches to problem-solving as well. We used HeFTy v1.8.3 to construct time–temperature paths of the plutons. The Monte Carlo inversion search method and Ketcham et al. (2007)'s annealing model were used. The zeta equivalent calibration was put as $\zeta = 1586.7$, $\sigma = 26.1$. Figures 4-6 show the Time–Temperature History window in HeFTy containing the results of inversion modeling that successfully found 1000 acceptable thermal histories. The measured and modeled track length of the studied samples are short (<14 μm) giving a relatively narrow distribution and are not bimodal. The time-temperature path of the Bozqush samples shows a relatively rapid initial cooling followed by long residence at the PAZ temperature (~60 to ~95 °C) (Fig 4).

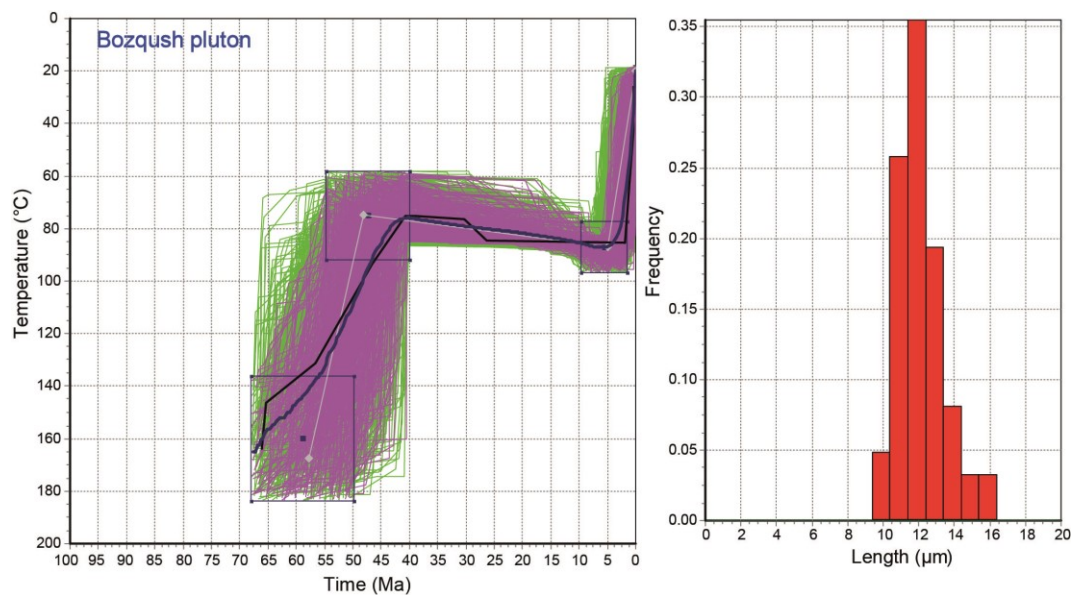


Fig 4. Monte Carlo inverse thermal history models for the Bozqush pluton using HeFTy (v1.8.3). The left panel shows time-temperature paths explored by the 1000 acceptable paths, green curves. The purple, black, and blue curves show 'good paths', 'best fit line', and 'weighted mean path', respectively. The numbers of total and good paths are 13112 and 434, respectively. The right panel shows the measured length histograms. See text for details.

The modeled time-temperature path show a rapid recent cooling from ~95 °C to the surface temperature, which was occurred about 5 Myrs. The time-temperature curve of the Kaleybar samples begins with a rapid initial cooling (Fig 5). The Figure (5) shows that the studied apatites were spent long time through the PAZ and slightly undergone heating from ~55 to ~95 °C. The last part of the curve shows a rapid recent cooling from ~95 °C to the surface temperature, which was started about 5 Ma ago. The time-temperature path of the Razgah samples exhibits a rapid first cooling followed by long

residence between ~55 to ~90 °C (Fig 6). The latest stage of cooling for the Razgah samples was occurred about 6 Myrs.

The first cooling ages can be corresponding to intrusive event (based on the good paths, 40-55 Ma for the Bozqush pluton, and 55-65 Ma for the Kaleybar and Razgah plutons), while the apparent ages closely approximates the mean time of the heating stage (Fig 4-6 and Table 2).

Table 2. Measured and modeled age and track length of the studied apatites using HeFTy (v1.8.3) software with GOF, goodness of fit.

	Bozqush	Kaleybar	Razgah
Model age	22.8	33.0	32.1
Measured age	22.8±1.5	33.0±2.9	32.1±1.2
GOF	1.00	1.00	1.00
Old age	50.6	62.3	61.1
Model track length	11.94±1.32	12.09±1.27	12.11±1.22
Measured track length	11.74±1.26	11.76±1.04	11.91±1.16
GOF	0.99	0.95	0.76

The resulting time-temperature history needs to be considered in conjunction with the available geological data. The KRB alkaline plutons were probably intruded at 30-50 Ma (based on dating of the shoshonitic magmatism, second magmatic cycle in NW Iran), which is consistent with the first cooling ages. Regionally

consistent AFT ages most likely indicate the time of final cooling and exhumation rather than later perturbations from volcanic activity or other thermal events. If the samples in question are in an active magmatic province, the AFT age and track length characteristics and the pressure-temperature-time history of the rocks can be compared with known parameters (age, thickness, and location of volcanic deposits or intrusions) to assess quantitatively whether magmatic reheating was likely, or whether reheating was associated with reburial (Fayon and Whitney 2007). Based on the present data such as the thermobarometry of clinopyroxenes and amphiboles, the occurrence of pseudoleucite, and the formation of porphyritic texture, the KRB plutons intruded into the Late Cretaceous and Eocene sedimentary and volcanic rocks at shallow levels of the crust and formed as sub-volcanic intrusions rather than deep plutonic bodies (Ashrafi 2009; Ashrafi et al. 2014). Therefore, the cooling of samples was possibly complex, as the short mean track lengths of samples showed.

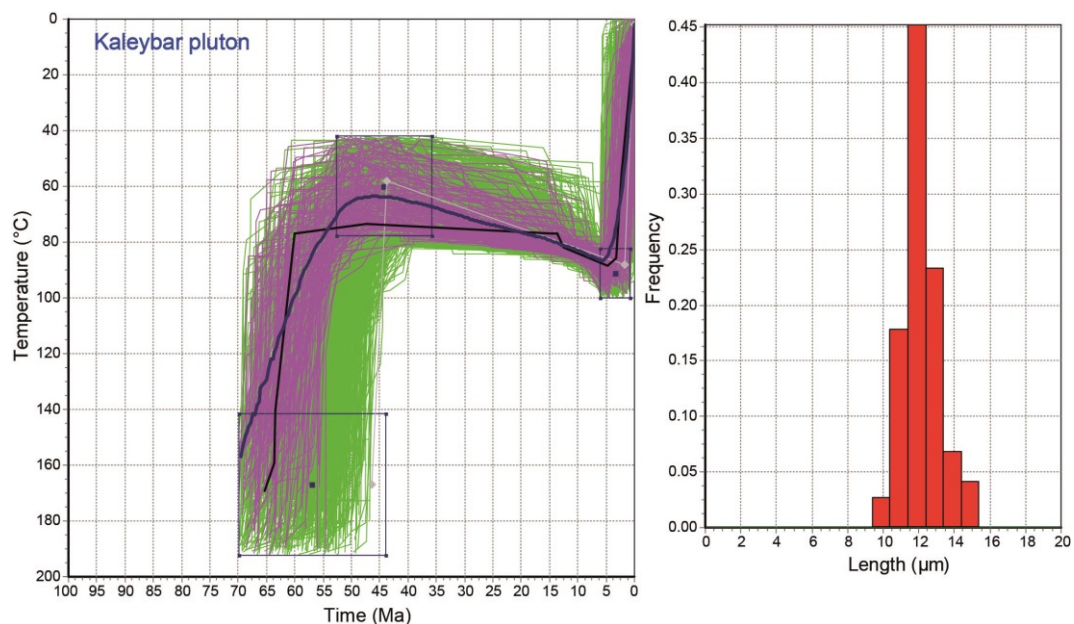


Fig 5. Monte Carlo inverse thermal history models for the Kaleybar pluton using HeFTy (v1.8.3). The left panel shows time-temperature paths explored by the 1000 acceptable paths. The legend of curves is the same as Figure 4. The numbers of total and good paths are 12726 and 159, respectively. The right panel shows the measured length histograms. See text for details.

The AFT ages are possibly affected by the recent exhumation of the KRB rocks. The amount of exhumation may vary locally reflecting different materials to be eroded (Hasebe and Hoshino 2003). The younger AFT age of the Bozqush pluton can be related to its totally igneous cover because the Kaleybar pluton and probably the Razgah pluton had the sedimentary-igneous cover (a differential exhumation). However, to understand the effect of different geology on the exhumation, the surrounding rocks of the KRB intrusions should be dated by the AFT method.

The studied samples are located in magmatically and tectonically active region. Thus, apatite fission tracks can be annealed and the ages reset, by a variety of thermal events such as tectonic activity (faulting, burial), and magmatism (volcanism, hydrothermal activity, intrusion). According to the stratigraphic age of the intrusions, the AFT ages were not probably reset at least for the Razgah and Kaleybar intrusions. Though, more data, such as absolute age of KRB rocks, detailed radiometric data, and dating by other thermochronometric system, is needed to constrain of

the precious time of final cooling and exhumation and

the possibility of later perturbations by thermal events.

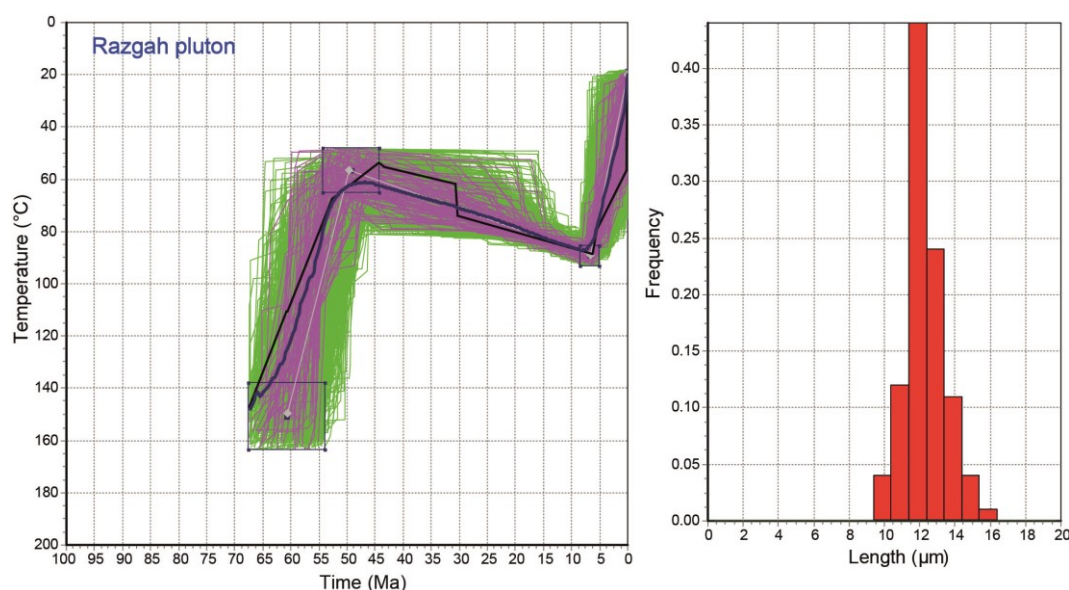


Fig 6. Monte Carlo inverse thermal history models for the Razgah pluton using HeFTy (v1.8.3). The left panel shows time-temperature paths explored by the 1000 acceptable paths. The legend of curves is the same as Figure 4. The numbers of total and good paths are 14568 and 108, respectively. The right panel shows the measured length histograms. See text for details.

6. Conclusion

The obtained AFT ages, ~29- 40 Ma, approximately in concordance with the shoshonitic magmatic cycle of NW Iran, indicate cooling of the KRB rocks to temperatures 110–60 °C, although the geological processes associated with this cooling may be open to question.

The KRB rocks are situated in a region with younger magmatism, and were formed as sub-volcanic intrusions. Thus, the cooling of samples was probably complex. However, the time-temperature graphs show that the studied samples were spent long time through the PAZ and slightly undergone heating. The first cooling ages can be corresponding to intrusive event (40-65 Ma), while the apparent ages closely approximate the mean time of the heating stage. The start of rapid recent cooling, from ~95° C to surface temperature, was occurred about 5 Ma ago. The AFT age of Bozqush pluton is younger (~29 Ma) than the others, which can be related to differential exhumation. Based on the geological evidence, totally igneous cover of the Bozqush area versus sedimentary-igneous cover of the Kaleybar and Razgah area, it infers a slower exhumation rate for the Bozqush area.

Acknowledgements

This work was supported by the Payame Noor and Tabriz Universities (Iran) and the Kanazawa University (Japan), for which we are thankful. The authors would like to acknowledge contributions of the IJES reviewers in improving the manuscript by providing valuable suggestions.

References

- Aghanabati A (1990) Magmatic rocks of Iran, Geological Quadrangle Map 1/2500000, Geological Survey of Iran, Tehran.
- Ahmadzadeh G, Jahangiri A, Lentz D, Mojtahedi M (2010) Petrogenesis of Plio-Quaternary post-collisional ultrapotassic volcanism in NW of Marand, NW Iran, *Journal of Asian Earth Sciences* 39: 37–50.
- Alavi M (1991) Tectonic Map of the Middle East 1/5000000, Geological Survey of Iran, Tehran.
- Alavi M (1996) Tectonostratigraphic Synthesis and Structural Style of the Alborz Mountain System in Iran, *Journal of Geodynamics* 21: 1-33.
- Alberti AA, Comin-Chiaromonte P, DiBattistini G, Nicoletti M, Petrucciani C, Sinigoi S (1976) Geochronology of the Eastern Azerbaijan Volcanic Plateau (northwest Iran), *Rendiconti della Societa Italiana di Mineralogia e Petrologia* 32: 579-590.
- Ashrafi N (2004) Petrological and geochemical investigations of the Razgah intrusion, East Azerbaijan, NW Iran, Unpublished MSc Thesis, Geology Department, University of Tabriz, Iran, (in Persian) 97 p.
- Ashrafi N (2009) Mineralogy, petrology, and geochemistry of foid-syenites of East Azerbaijan, NW Iran, Unpublished PhD Thesis, Geology Department, University of Tabriz, Iran, (in Persian) 190 p.
- Ashrafi N, Jahangiri A, Hasebe N (2014) Study of amphibole and clinopyroxene chemistry of the Bozqush, Kaleybar, and Razgah alkaline igneous intrusions, NW Iran, *Iranian Journal of Crystallography and Mineralogy* (in Persian) 3: 381-392.

- Axen GJ, Lam PJ, Grove M, Stockli DF, Hassanzadeh J (2001) Exhumation of the west-central Alborz mountains, Iran, Caspian subsidence, and collision-related tectonics, *Geology* 29: 559–562.
- Babakhani AR, Lesquyer JL, Riou R (1990) Explanatory text of Ahar, Geological Quadrangle Map 1/250000, Geological Survey of Iran, Tehran.
- Ballato P, Stockli DF, Ghassemi MR, Landgraf A, Strecker MR, Hassanzadeh J, Friedrich A, Tabatabaei SH (2012) Accommodation of transpressional strain in the Arabia-Eurasia collision zone: new constraints from (U-Th)/He thermochronology in the Alborz mountains, N Iran, *Tectonics* 32: 1–18.
- Barbarand J, Carter A, Wood IG, Hurford AJ (2003) Compositional and structural control of fission-track annealing in apatite, *Chemical Geology* 198:107–137.
- Barfod GH, Otero O, Albarède F (2003) Phosphate Lu-Hf geochronology, *Chemical Geology* 200: 241–253.
- Carlson WD, Donelick RA, Ketcham RA (1999) Variability of apatite fission-track annealing kinetics I: Experimental results, *American Mineralogist* 84: 1213–1223.
- Carter A (1999) Present status and future avenues of source region discrimination and characterization using fission track analysis, *Sedimentary Geology* 124: 31–45.
- Castro A, Aghazadeh M, Badrzadeh Z, Chichorro M (2013) Late Eocene–Oligocene post-collisional monzonitic intrusions from the Alborz magmatic belt, NW Iran: An example of monzonite magma generation from a metasomatized mantle source, *Lithos* 180–181: 109–127.
- Chamberlain KR, Bowring SA (2000) Apatite-feldspar U–Pb thermochronometer: A reliable, mid-range (450°C), diffusion-controlled system, *Chemical Geology* 172: 173–200.
- Chew DM, Donelick RA (2012) Combined apatite fission track and U–Pb dating by LA–ICP–MS and its application in apatite provenance analysis, *Mineralogical Association of Canada Short Course* 42: 219–247.
- Comin-Chiaromonti P, Meriani S, Mosca R, Sinigoi S (1979) On the occurrence of analcime in the northeastern Azerbaijan volcanic rocks (north western Iran), *Lithos* 12: 187–198.
- Comin-Chiaromonti P, Nardin G, Sinigoi S (1975) The alkali quartz-trachytes of the Gasr Dagh (Azerbaijan, northwest Iran), *Rendiconti della Società Italiana di Mineralogia e Petrologia* 31: 297–308.
- Cox R, Kosler J, Sylvester P, Hodych J, (2000) Apatite fission track (FT) dating by LAM-ICO-MS analysis, Abstract of Goldschmidt 2000, Journal of Conference Abstracts 5: 322.
- Dabiri R, Emami MH, Mollai H, Chen B, Vosogi-Abedini M, Rashidnejad-Omran N, Ghaffari M (2011) Quaternary post-collision alkaline volcanism NW of Ahar (NW Iran): Geochemical constraints of fractional crystallization process, *Geologica Carpathica* 62: 547–562.
- Didon J, Gemain YM (1976) Le Sabalan, Volcan Plio-Quaternaire de l’Azerbaïdjan oriental (Iran): Étude géologique et pétrographique de l’édifice et de son environnement régional, PhD thesis, University of Grenoble, France.
- Donelick RA, O’Sullivan PB, Ketcham RA (2005) Apatite fission-track analysis, In: Low-Temperature Thermochronology: Techniques, Interpretations, and Applications (Eds. Reiners PW and Ehlers TA), *Reviews in Mineralogy and Geochemistry* 58: 49–94.
- Farley KA (2000) Helium diffusion from apatite: General behavior as illustrated by Durango fluorapatite, *Journal of Geophysical Research* 105: 2903–2914.
- Fayon AK, Whitney DL (2007) Interpretation of tectonic versus magmatic processes for resetting apatite fission track ages in the Niğde Massif, Turkey, *Tectonophysics* 434: 1–13.
- Fitzgerald PG, Sorkhabi RB, Redfield TF (1995) Uplift and denudation of the central Alaska range: a case study in the use of apatite fission track thermochronology to determine absolute uplift parameters, *Journal of Geophysical Research* 100: 20175–20191.
- Foster GL, Vance D (2006) In situ Nd isotopic analysis of geological materials by laser ablation MC-ICP-MS, *Journal of Analytical Atomic Spectrometry* 21: 288–296.
- Galbraith RF (1981) On statistical models for fission track counts, *Mathematical Geology* 13:471–488.
- Gallagher K (1995) Evolving temperature histories from apatite fission-track data, *Earth and Planetary Science Letters* 136: 421–435.
- Gallagher K, Hawkesworth CJ, Mantovani MSM (1994) The denudation history of the onshore continental margin of SE Brazil inferred from apatite fission-track data, *Journal of Geophysical Research* 99: 18117–18145.
- Ghorbani M (2011) Magmatism and alteration with regards to mineralization of the Ahar-Jolfa belt (Arasbaran), *Journal of Basic Sciences of Islamic Azad University* (in Persian) 21: 23–28.
- Gleadow AJW (1981) Fission-track dating methods: what are the real alternatives? *Nuclear Tracks* 5:3–14.
- Gleadow AJW, Duddy IR, Green PF, Hegarty KA (1986a) Fission-track lengths in the apatite annealing zone and the interpretation of mixed ages, *Earth and Planetary Science Letters* 78: 245–254.
- Gleadow AJW, Duddy IR, Green PF, Lovering JF (1986b) Confined fission track lengths in apatite: a diagnostic tool for thermal history analysis, *Contribution to Mineralogy and Petrology* 94: 405–415.
- Green PF, Duddy IR, Gleadow AJW, Lovering JF (1989) Apatite fission-track analysis as a paleotemperature indicator for hydrocarbon

- exploration, In: Thermal history of sedimentary basins; methods and case histories (Eds. Naeser ND and McCulloh TH) 181-195, Springer-Verlag, New York.
- Green PF, Duddy IR, Gleadow AJW, Tingate PR, Laslett GM (1986) Thermal annealing of fission tracks in apatite: I. A qualitative description, *Chemical Geology, Isotope Geoscience Section* 59: 237–253.
- Gregory CJ, Mcfarlane CRM, Hermann J, Rubatto D (2009) Tracing the evolution of calc-alkaline magmas: In-situ Sm-Nd isotope studies of accessory minerals in the Bergell Igneous Complex, Italy, *Chemical Geology* 260: 73-86.
- Guest B, Stockli DF, Grove M, Axen GJ, Lam PS, Hassanzadeh J (2006) Thermal histories from the central Alborz mountains, northern Iran: Implications for the spatial and temporal distribution of deformation in northern Iran, *Geological Society of America Bulletin* 118:1507–1521.
- Hasebe N, Barbarand J, Jarvis K, Carter A, Hurford AJ (2004) Apatite fission-track chronometry using laser ablation ICP-MS, *Chemical Geology* 207: 135-145.
- Hasebe N, Hoshino H (2003) Igneous rocks emplacement and exhumation of sedimentary basement: Fission track age determination on the Osuzuyama volcano-plutonic complex and surrounding rocks, Miyazaki prefecture, Southwest Japan, *Geochemical Journal* 37: 537-543.
- Hasebe N, Tamura A, Arai S (2013) Zeta equivalent fission-track dating using LA-ICP-MS and examples with simultaneous U–Pb dating, *Island Arc* 22: 280-291.
- Hurford AJ, Green PF (1982) A user's guide to fission track dating calibration, *Earth and Planetary Science Letters* 59: 343–354.
- Hurford AJ, Green PF (1983) The zeta age calibration of fission track dating, *Isotope Geosciences* 1:285–317.
- Jaffey AH, Flynn KF, Glendenin LE, Bentley WC, Essling AM (1971) Precision measurement of the half-lives and specific activities of ^{235}U and ^{238}U , *Physical Review* 4: 1889-1906.
- Jahangiri A (2007) Post-collisional Miocene adakitic volcanism in NW Iran: geochemical and geodynamic implications, *Journal of Asian Earth Sciences* 30: 433–447.
- Jarvis KE, Williams JG (1993) Laser ablation inductively coupled plasma mass spectrometry (LA-ICP-MS): a rapid technique for the direct, quantitative determination of major, trace and rare-earth elements in geological samples, *Chemical Geology* 106: 251–262.
- Ketcham RA (2005) Forward and inverse modeling of low-temperature thermochronometry data, *Reviews in Mineralogy and Geochemistry* 58: 275-314.
- Ketcham RA, Carter A, Donelick RA, Barbarand J, Hurford AJ (2007) Improved measurement of fission-track annealing in apatite using c-axis projection, *American Mineralogist* 92: 789-798.
- Ketcham RA, Donelick RA, Donelick MB (2000) AFTSolve: A program for multi-kinetic modeling of apatite fission-track data, *Geological Materials Research* 2: 1-32
- Kohn BP, Green PF (2002) Low Temperature Thermochronology: from Tectonics to Landscape Evolution, *Tectonophysics* 349: 1-4.
- Laslett GM, Green PF, Duddy IR, Gleadow AJW (1987) Thermal annealing of fission tracks in apatite, II: A quantitative analysis, *Chemical Geology* 65: 1-3.
- Le Maitre RW, Streckeisen A, Zanettin B, Le Bas MJ, Bonin B, Bateman P, Bellieni G, Dudek A, Efremova SA, Keller J, Lameyre J, Sabine PA, Schmid R, Sørensen H, Woolley AR (2002) Igneous rocks: a classification glossary of terms, Cambridge University Press, Cambridge, 236 p.
- Mohajjel M, Fergusson CL, Sahandi MR (2003) Cretaceous-Tertiary convergence and continental collision, Sanandaj-Sirjan Zone, western Iran, *Journal of Asian Earth Sciences* 21: 397–412.
- Moine-Vaziri H (1999) An introduction to the magmatism in Iran, Second Edition, Tarbiat Moalem University Publication, Tehran (in Persian) 440 p.
- Mollai H, Pe-Piper G, Dabiri R (2014) Genetic relationships between skarn ore deposits and magmatic activity in the Ahar region, Western Alborz, NW Iran: Evidence for metasomatism and copper mineralization, *Geologica Carpathica* 65: 207–225.
- Nabatian G, Ghaderi M, Neubauer F, Honarmand M, Liu X, Dong Y, Jiang SY, Quadt A, Bernroider M (2014) Petrogenesis of Tarom high-potassic granitoids in the Alborz–Azarbaijan belt, Iran: Geochemical, U–Pb zircon and Sr–Nd–Pb isotopic constraints, *Lithos* 184–187: 324-345.
- Pearce NJG, Perkins WT, Westgate JA, Gorton MP, Jackson SE, Neal CR, Chenery SP (1997) A compilation of new and published major and trace element data for NIST SRM 610 and NIST SRM 612 glass reference materials, *Geostandards Newsletter* 21: 115-144.
- Rezaeian M, Carter A, Hovius N, Allen MB (2012) Cenozoic exhumation history of the Alborz Mountains, Iran: New constraints from low-temperature chronometry, *Tectonics* 31, TC2004, doi:10.1029/2011TC002974.
- Schoene B, Bowring SA (2007) Determining accurate temperature-time paths from U–Pb thermochronology: An example from the Kaapvaal craton, southern Africa, *Geochimica et Cosmochimica Acta* 71: 165-185.
- Shafaii-Moghadam H, Ghorbani G, Zaki Khedr M, Fazlnia N, Chiaradia M, Eyuboglu Y, Santosh M, Galindo Francisco C, Lopez Martinez M, Gourgau A, Arai S (2014) Late Miocene K-rich volcanism in the Eslamieh Peninsula (Saray), NW Iran: Implications for geodynamic evolution of the Turkish–Iranian High Plateau, *Gondwana Research* 26: 1028-1050.

Spadavecchia A, Hahn B (1967) Die Rotationskammer und einige Anwendungen, *Helvetica Physica Acta* 40: 1063-1079.

Stöcklin J, Nabavi MH (1973) Tectonic map of Iran 1/2500000, Geological Survey of Iran, Teheran.

Svojtka M, Kosler M, (2002) Fission-track dating of zircon by laser ablation ICPMS, Abstracts of the 12th annual VM Goldschmidt Conference, Davos,

Switzerland, Special Supplement of *Geochimica et Cosmochimica Acta* vol. 66, p. A756.

Tajbakhsh Gh, Emami MH, Moine-Vaziri H, Rashidnejad-Omran N (2012) Petrology, geochemistry and tectonomagmatic setting of Kaleybar intrusion (Eastern Azarbaijan), *Iranian Scientific Quarterly Journal, Geosciences* 22: 205-224 (in Persian).